Nuclear stopping power at ~15 GeV/nucleon

Scott Chapman and Miklos Gyulassy
Nuclear Science Division, Lawrence Berkeley Laboratory, Berkeley, California 94720
(Received 12 November 1991)

Fireball, firestreak, and hadronic string models are shown to overpredict recent central 15A GeV Si+Au E802 spectrometer data. Claims in the literature about full nuclear stopping in Si+Au reactions are therefore not supported by these data. In fact, fits to the spectrometer data indicate that up to half of the projectile nucleons may lose less than one unit of rapidity after traversing 5–10 fm of nuclear matter, implying an unexpected long stopping length of ~20 fm. On the other hand, E810, E814, and preliminary E802 $dN_{\rm ch}/d\eta$ data are more consistent with the expected degree of stopping.

PACS number(s): 25.75.+r, 24.10.−i, 13.85.Ni

I. INTRODUCTION

It has been claimed that "full stopping is realized [1–4], showing a behavior close to the landau model [5] and to relativistic fluid dynamics [6], and the energy density can reach values comparable to the critical values for QGP formation" [7]. However, as we pointed out in Ref. [8], the published E802 spectrometer data [9] cast doubt on this belief, since in fact none of the present models is consistent with the full array of data. Moreover, if the spectrometer dN/dy are normalized correctly, then these data are more indicative of a surprising degree of nuclear transparency. On the other hand, $dN_{\rm ch}/d\eta$ [10] and high-rapidity E810 [11] and E814 [12] data are well reproduced by models incorporating a high degree of nuclear stopping. As a result of this apparent inconsistency, no firm conclusion can yet be drawn on the important topic of the amount of nuclear stopping at the Brookhaven Alternating Gradient Synchrotron (AGS).

In our letter [8] we discussed a model-independent fit to the spectrometer data which showed that if systematic errors do not cause more than a 30% suppression of proton and pion yields, then four-momentum and baryon conservation laws imply that at least 11 out of 28 projectile nucleons suffer less than one unit of rapidity loss during a central Si+Au collision. In this paper, we give the precise functional form of the fit used in the Letter, as well as introducing three other fits which allow for the possibility of systematic errors in excess of 30%. In addition to E802 spectrometer data [9], we compare these four fits to E802 $dN_{\rm ch}/d\eta$ data [10] as well as data from the E810 [11] and E814 [12] Collaborations. In our Letter, we developed a multicomponent model (mcm) in order to quantify the amount of nuclear stopping implied by the E802 spectrometer data. In this paper, in addition to explaining the mcm in more detail in the Appendix, we show that a simpler double firestreak model leads to similar conclusions about the amount of stopping. These types of models are only able to reproduce the spectrometer data with stopping lengths of ~20 fm. In addition to central Si+Au data, we discuss the agreement of these models with unpublished preliminary central Si+Al and Si+Cu E802 spectrometer data [13], and make predictions for central Au+Au proton and pion distributions at these same energies. The long stopping lengths implied by the E802 spectrometer data provide a sharp contrast to the results of $p+p$ and $p+A$ experiments at these same energies which imply stopping lengths of more on the order of 8–10 fm [14]. Thus, either something new and unexplained is occurring in central Si+Au collisions at the AGS or else systematic errors in the spectrometer dN/dy data must be significantly larger than previously estimated. In any case, the published E802 spectrometer data do not support claims of full nuclear stopping which are prevalent in the literature [1–5,7,15–19].

II. THE HADRONIC FIREBALL

In the generic hadronic fireball model [20], the projectile nucleus is assumed to be completely stopped by the target nucleus in the participant center-of-mass frame, whereupon thermal and chemical equilibrium are established. By treating both nuclei as hard spheres of constant baryon density ($\rho_0=0.145$ fm^{-3}), geometry determines the number of interacting nucleons for any given impact parameter. For example, in a $b=0$ Si+Au collision, all 28 ($=N_p$) silicon nucleons interact with a central tube of about 75 ($=N_t$) gold nucleons, thus making the baryon number of the resulting fireball 103 ($=N_f$). The remaining 122 gold nucleons of this example are merely spectators which are ignored in this model. Once N_p and N_t are known, the rapidity of the fireball rest frame and the total fireball energy in that frame are fixed by kinematics. For the Si+Au example with $y_{p0}=3.4$ and $y_{t0}=0$, $y_f=1.3$ and $E_f=250$ GeV.

After its creation, the fireball expands and cools until freeze-out, when the mean free path of the fireball hadrons becomes approximately the same size as the radius of the fireball. The temperature and chemical potentials at freeze-out define the particle distributions according to

$$f_i=\frac{d^3N_i}{dy\,d^2p_\perp}=\frac{\gamma_i g_i V_{\rm fr} E}{\exp[(E-B_i\mu-S_i\mu_s)/T]-(-1)^{B_i}}\,, \tag{1}$$

where B_i, S_i, and g_i are the baryon number, strangeness, and spin-isospin multiplicity for each species of hadron, $V_{\rm fr}$ is the freeze-out volume, and γ_i is a parameter introduced to allow for the incomplete chemical equilibration. We assume that $\gamma_i=\gamma_s$ for all strange hadrons and $\gamma_i=1$ for all other hadrons. Since E_f and N_f are fixed by kinematics, T, μ, and μ_s can be found by choosing values for γ_s and $V_{\rm fr}$ (or $\rho_{\rm fr}=N_f/V_{\rm fr}$) and then solving the following integral equations:

$$E_f=\sum_{i=\text{hadrons}}\int d^2p_\perp dy\, Ef_i\ , \tag{2}$$

$$N_f=\sum_{i=\text{baryons}} B_i\int d^2p_\perp dy\, f_i\ , \tag{3}$$

$$0=\sum_{i=\text{strange}} S_i\int d^2p_\perp dy\, f_i\ . \tag{4}$$

We treat explicitly only the following hadronic resonances: $N,\Delta,\Lambda,\Sigma,\pi,\eta,\rho,\omega,\eta',K,K^*$, and their antiparticles. For example, for $b=0$, $\lambda_s=0.5$, and $\rho_{\rm fr}=5\rho_0$, we find that $T=200$ MeV, $\mu=418$ MeV, and $\mu_s=92$ MeV for AGS energy.

Once, T, μ, and μ_s have been found for a given set of input parameters, $f_i(y,p_\perp)$ determine the invariant distributions for each species of hadron in the fireball. However, before reaching the detector, the heavy baryon and meson resonances decay as follows: $\Delta\to N+\pi$, $\Lambda\to p+\pi^-$ (64% of the time), $\Sigma^+\to p+\pi^0$ (52%), $\Sigma^+\to n+\pi^+$ (48%), $\Sigma^0\to p+\pi^-$ (64%), $\Sigma^-\to n+\pi^-$, $\eta\to 3\pi$ (30%), $\rho\to 2\pi$, $\omega\to 3\pi$(90%), $\eta'\to 2\pi$, and $K^*\to K+\pi$, where the balance of the Λ, Σ^0, η, and ω decays are into undetected neutrals. For the 3π decays, it is assumed for simplicity that each daughter particle carries away $\frac{1}{3}$ of the parent energy. By convoluting the above decays with parent distribution functions as in Ref. [21], the resonance contributions to the nucleon and pion distributions are found.

The net charge/baryon of the fireball is given by

$$(Z/A)_f=\frac{(Z_p/A_p)N_p+(Z_t/A_t)N_t}{N_f}\ , \tag{5}$$

where Z_p (Z_t) and A_p (A_t) are the charge and atomic number of the projectile (target) nucleus. Charge conservation is enforced as follows: All final state mesons not coming from strange baryon decays are assumed to be distributed isosymmetrically, and therefore the net charge carried by these mesons is determined solely by the kaon abundances:

$$C_{\rm mes}=N_{K^+}-N_{K^-}\ . \tag{6}$$

From isosymmetry ($N_{K^0}-N_{K^+}$, etc.) and conservation of strangeness before strange baryon decays, we have the relation $C_{\rm mes}=0.5Y$, where Y is the number of strange baryons in the fireball. It is assumed that all of the strange baryons have the same mass (1.17 GeV) so that their relative abundances before decay do not depend on the temperature or chemical potentials. These abundances are taken to be $\frac{1}{4}$, $\frac{1}{2}(Z/A)_f$, $\frac{1}{4}$, and $\frac{1}{2}[1-(Z/A)_f]$ for Λ, Σ^+, Σ^0, and Σ^-, respectively. In this way, the net charge/baryon of all strange hadrons is always identical to the incoming charge/baryon ratio of $(Z/A)_f$. If, on the other hand, we had chosen Λ's and Σ's to have different masses, we would need to introduce either another chemical potential or some more complicated prescription for choosing strange baryon abundances in order to enforce charge conservation for arbitrary T, μ, and μ_s. Finally, by demanding that $(Z/A)_f$ of the final nucleons not coming from strange baryon decays be protons, overall charge conservation can be enforced.

In the E802 experiment [9], central Si+Au events were identified by a high multiplicity trigger whose cross section ($=\sigma_{\rm cent}$) represented 7% of the total Si+Au inelastic cross section ($=3822$ mb [13]). In our model, we chose a maximum impact parameter ($b_{\rm max}=2.9$ fm) such that $\pi b_{\rm max}^2=\sigma_{\rm cent}$ and then integrated our fireball results over b from 0 to $b_{\rm max}$.

In the experiment, measurements were made using a spectrometer arm with a range of $5^\circ<\theta<55^\circ$ which could detect and identify charged particles with total momentum between 0.5 and 3 GeV/c [9,22]. The resulting raw particle distributions were binned both in y and $m_\perp$. For each rapidity bin, the distributions appear to be well fit by pure exponentials in $m_\perp$ [9]:

$$d^3N_i/dy\,d^2m_\perp=\rho_i(y)\exp[-(m_{i\perp}-m_i)/T_i(y)]\ . \tag{7}$$

The rapidity distributions were then estimated by integrating these fits over $m_\perp$:

$$dN_i/dy=2\pi\rho_i(y)T_i(y)[T_i(y)+m_i]\ . \tag{8}$$

In the fireball model, dN_i/dy can be calculated in two ways: by numerically integrating f_i over all $d^2m_\perp$ or by using the exponential fitting procedure outlined above after imposing the experimental phase space constraints. For all of our calculations, the difference between the results of these two methods was less than 20% for dN_π/dy and completely negligible for dN_p/dy.

In Fig. 1 we compare three fireball models to the data. The solid dots are data from the E802 spectrometer [9], while the diamonds and squares are data from E810 [11] and E814 [12], respectively. It should be noted that the E814 data are actually for Si+Pb collisions rather than Si+Au and that the three experiments use different centrality triggers (the E810 trigger has twice the cross section of the E802 trigger, while the E814 trigger has less than half the cross section of E802). Nevertheless, comparing these data sets to one another is done quite often [23] and is useful for making qualitative cross checks. The solid line in Fig. 1 shows the results of the generic fireball model outlined above with $\rho_{\rm fr}=5\rho_0$ and $\gamma_s=0.5$. This fireball model produces more than a factor of 2 too many protons, pions, and kaons (not shown) at midrapidity. Using a higher freeze-out baryon density results in more heavy baryon resonances and slightly fewer pions, but the increased temperature makes the distributions become too broad in $m_\perp$. Increasing (decreasing) γ_s increases (decreases) the number of kaons and strange

baryons but does not have a significant effect on the total number of midrapidity protons and pions. In fact, no reasonable variation of $\rho_{\rm fr}$ and/or γ_s significantly improves agreement with the data. In addition to the generic fireball, Fig. 1 also shows results from the Landau hydrodynamic longitudinally expanding fireball [5] (dashed line) and the hydrochemical spherically expanding fireball [18,19] (dot-dashed line). The longitudinal expansion of the Landau fireball reduces the midrapidity proton and pion peaks but still overpredicts the E802 proton data by at least 70% in the range $1.5 < y < 2$. On the other hand, it should be noted that this model does a very good job of reproducing high-rapidity E810 and E814 data. Even though the spherical expansion of the hydrochemical model provides a possible explanation for the difference in proton and pion slopes, this model also fails to reproduce the measured norms of these distributions. In fact, all of the fireball models considered here overpredict the E802 proton and/or pion rapidity distributions by at least 70% in some rapidity range.

It has been suggested [18,19] that at least some of the discrepancy in dN_π/dy could be due to an unmeasured excess of low $p_\perp$ pions coming from baryon resonance decays. The dot-dot-dashed curves in the bottom two panels of Fig. 1 show the distributions of protons and pions coming only from baryon resonance decays in the generic fireball model. At least for the generic fireball, any low $p_\perp$ enhancement due to these resonances is entirely negligible for protons and less than 20% for pions, as can be seen by comparing the restricted, exponentially fitted dN_π/dy (dot-dot-dashed line in Fig. 1) with the directly calculated dN_π/dy (solid line). Furthermore, even if one makes the assumption of the hydrochemical model [18,19] that none of the pions coming from baryon resonance decays are detected, fireball models still predict 70% more midrapidity pions than are seen in the data (dot-dashed line in Fig. 1). Since none of the fireball models discussed here can simultaneously reproduce all of the data, we turn to other models.

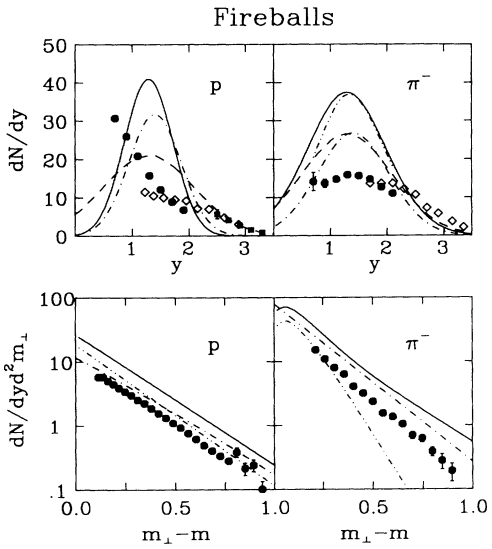

FIG. 1. The solid dots in the upper panels show the proton and π^- rapidity distributions measured by the E802 spectrometer in 14.6A GeV/c central Si+Au reactions, while the bottom panels show the $m_\perp$ distributions for $y=1.3$ in those same reactions [9]. The diamonds show E810 "+"-"−" and negatively charged particle distributions for Si+Au using a trigger with twice the cross section of the E802 central trigger [11]. The solid squares are E814 proton data for central Si+Pb reactions [12]. Solid curves show results of the generic fireball model, while dashed and dot-dashed curves denote Landau hydrodynamic fireball [5] and hydrochemical fireball [18,19] results, respectively. The norms of the hydrochemical results have been adjusted in accordance with the published erratum [19]. The dot-dot-dashed curves in the lower panels show $m_\perp$ distributions of protons and π^-'s coming only from heavy baryon decays in the generic fireball model. The dot-dot-dashed curve in the upper right panel shows the generic fireball prediction for the pion rapidity distribution given the restricted phase space of the experiment.

III. THE FIRESTREAK AND STRING MODELS

The firestreak [20,24] model was designed to take into account the diffuse edges of colliding nuclei by creating many smaller scale regions of local equilibrium rather than a single large fireball. In this model, the projectile and target nuclei are divided into longitudinal tubes with transverse area $a_\perp$ ($\lesssim 1$ fm^2). Each set of two opposing tubes forms a completely stopped miniature fireball (or firestreak) in its local center-of-mass frame. In this way a large number of independent firestreaks forms, each with its own local values of N_f, y_f, T, μ, and μ_s. As a result of this locality, Woods-Saxon density distributions rather than sharp spheres can be used to determine how many nucleons are in each tube. Often, some very asymmetric cases will result. For example, a tube containing three nucleons from the center of a gold nucleus could interact with a tube containing 0.1 nucleon from the diffuse edge of a projectile silicon nucleus to create a streak with $N_f=3.1$ and $y_f=0.4$. These asymmetries provide a natural way to generate low-rapidity "spectator" contributions, even though there are no true spectators in this model.

Hadronic string models [25] also feature locality, though they do not impose the requirement of complete nuclear stopping. In Fig. 2, we compare the firestreak (dashes) and two string models [Attila [26] (solid) and quark-gluon-string model [7] (histogram)] with the data. For the firestreak and Attila models, we have calculated $T_i(y)$ via the exponential fitting procedure of Eq. (7) in order to compare our curves to the published $T_i(y)$ values. Though the firestreak improves on the fireball by showing "spectator" contributions, it still has the problem of predicting far too many midrapidity protons and pions, even after the experimental acceptance has been folded in (dot-dot-dashed line in dN_π/dy). The string models do a better job of reproducing the overall ramp shape of dN_p/dy, though they still overpredict by at least 70% the number of pions seen by E802. It should be noted that although Attila overpredicts by about 50% the high-rapidity protons seen by E802, it reproduces those

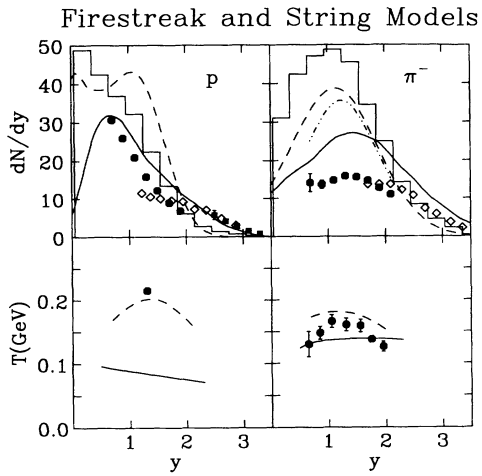

FIG. 2. The top panels are as in Fig. 1, while the bottom panels are the inverse slope parameters of Eq. (7) [9]. These data are compared to firestreak [24] (dashed), Attila [26] (solid), and QGSM [7] (histogram) calculations. The dot-dot-dashed curve in the upper right panel shows the firestreak prediction with experimental phase space restrictions.

seen by E810 and E814 very well.

Recently, there have been claims [27] that the relativistic quantum molecular dynamics model [15] is consistent to within 23% with the E802 spectrometer data. In Fig. 3, we compare various RQMD runs with proton and pion rapidity data. Since Sorge *et al.* have not yet published proton and π^- rapidity distributions in the same paper, we show the proton distribution from Ref. [28] (histogram) and the π^- distribution from Ref. [16] (solid curve). These curves consistently overpredict the E802 data, even by as much as 70% for midrapidity pions. The open circles in Fig. 3 represent the results of an RQMD run which was subjected to the E802 experimental acceptances and cuts [27]. It is interesting that this RQMD run still overpredicts the E802 pion and proton yields by ~50% and ~70%, respectively, in the region $1.5<y<2$. None of these discrepancies can be due to undetected low $p_\perp$ components since the same exponential fitting procedure was used for this RQMD run as for the E802 data. On the other hand, RQMD does a very good job of reproducing the high-rapidity E810 and E814 data.

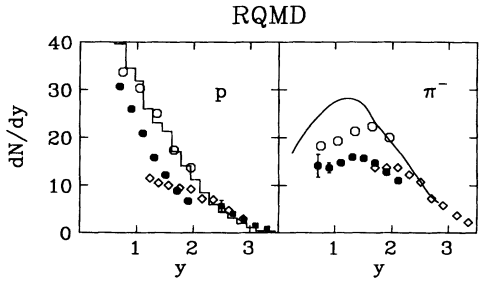

FIG. 3. The data of the top of Fig. 1 are compared to RQMD calculations by Sorge *et al.* (histogram [28] and solid [16]) and to RQMD calculations which have explicitly incorporated the experimental acceptances and cuts (open circles) [27].

IV. MODEL-INDEPENDENT FITS

Having seen that none of the above equilibrium and nonequilibrium models for nuclear collision dynamics are able to simultaneously reproduce all of the published data, we consider next a model-independent fitting procedure in order to isolate possible causes for the discrepancies. We begin by fitting the experimental $T_i(y)$ [13] and $(dN/dy)_i(y)$ [9] data with simple functions which have reasonable extrapolations to phase space regions outside of the experimental acceptance. Equations (7) and (8) are then used to determine the invariant distributions, $f_i = d^3N_i/dy\,d^2m_\perp$, from which information about momentum and energy conservation can be extracted.

For the meson $(dN/dy)_i(y)$ we use

$$(dN/dy)_i = \alpha C_i \exp[-(y-y_i)^2/\delta_i], \quad -1 \le y \le 4, \tag{9}$$

where (C_i, y_i, δ_i) are fit with (16,1.4,1), (16,1.35,1.3), (3.5,0.95,1), and (0.67,1.3,1) for π^+, π^-, K^+, and K^-, respectively. The reported data are fit with $\alpha=1$, but later we set $\alpha=1.3$ to account for experimental systematic errors. The meson and proton temperatures are given by

$$T_{\pi^+} = T_{\pi^-} = 0.06 + 0.1\exp[-(y-1.3)^2/1.2] + 0.03\exp(-y^2), \tag{10}$$

$$T_{K^+} = T_{K^-} = 0.19\exp[-(y-1.3)^2/2], \tag{11}$$

$$T_p = \begin{cases} 0.23\exp[-(y-1.55)^2] + 0.1\exp(-y^2), & y<2.2, \\ 0.15, & y>2.2. \end{cases} \tag{12}$$

We fitted the proton rapidity spectrum with a falling quadratic ramp and included adjustable undetected spectator and projectile Gaussians in order to conserve baryon number and to test for transparency:

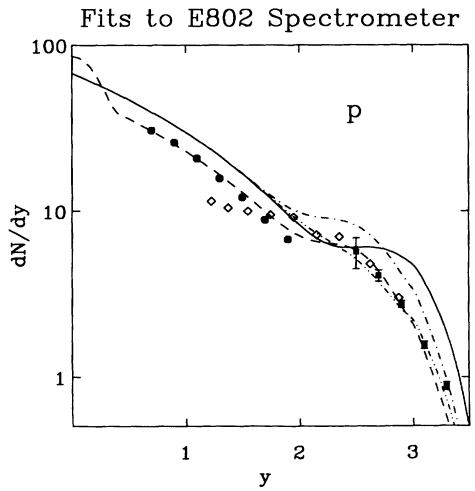

FIG. 4. The same proton data as in Fig. 1 plotted on a logarithmic scale. In addition to a data fit (dashed) which does not conserve four-momentum, we show fit 1 (solid), fit 2 (dot-dashed), fit 3 (dot-dashed), and fit 4 (dot-dot-dashed).

$$(dN/dy)_p=\alpha\times\begin{cases} C_{\rm spec}e^{(-y^2/\delta_{\rm spec})}, & -1<y<0 \\ \text{Max}\begin{bmatrix} C_{\rm spec}e^{(-y^2/\delta_{\rm spec})} \\ 6y^2-35y+52+C_{\rm pro}e^{[-(y-y_{\rm pro})^2/\delta_{\rm pro}]}\end{bmatrix}, & 0<y<3 \\ 7-2y+C_{\rm pro}e^{[-(y-y_{\rm pro})^2/\delta_{\rm pro}]}, & 3<y<3.5 \\ 0, \quad \text{otherwise}, \end{cases} \tag{13}$$

where $\delta_{\rm pro}=0.2$. For the unobserved neutral meson distributions it is assumed that $\pi^0=(\pi^++\pi^-)/2$, $K^0=K^+$, and $\bar{K}^0=K^-$. Charge conservation is enforced by demanding that the total number of final protons be $N_p=14+79-N_{\pi^+}-N_{K^+}+N_{\pi^-}+N_{K^-}$ (=91.9 for the above fit). We employ E810 and E814 data to guide our dN_p/dy extrapolation to high rapidities by using $(y_{\rm pro},C_{\rm pro},C_{\rm spec},\delta_{\rm spec})=$ data fit $=(2.5,3.8,80.9,0.17)$, where the last two parameters were chosen to get the right value for N_p. With N_p fixed, the total number of undetected neutrons is given by baryon number conservation, $N_n=28+197-N_p=133.1$. The correct value for N_n can be achieved by assuming an n/p ratio of 1.3 for $y>2$ (based on E814 findings [29]) and $n/p=1.46$ for $y<2$. This fit to the three experiments at the AGS allows us to take into account all of the observed energy in longitudinal and transverse motion as well as pion and kaon production. Data fit is shown by the dashed lines in Figs. 4, 5, and 6 (solid lines for the temperatures).

The total outgoing longitudinal momentum P_z implied by this fit is easily calculated by integrating $m_\perp\sinh(y)f_i$ over $d^2m_\perp$ and y:

$$P_z=\sum_{i=\text{hadrons}}\int dy\frac{2T_i^2+2T_im_i+m_i^2}{T_i+m_i}(dN/dy)_i\sinh(y)\ . \tag{14}$$

E is simply found by replacing $\sinh(y)$ by $\cosh(y)$. For data fit, the integration over y gives $P_z=289$ GeV/c and $E=495$ GeV, whereas the total incoming energy and momentum are known to be $P_z=409$ GeV/c $(=28\times14.6)$ and $E=595$ GeV $(=197\times0.939+28\times14.63)$. 120 GeV/$c$ of the incoming momentum and 100 GeV of the energy are unaccounted for in this fit to the data. If we assume that neither leptons nor photons carry a significant fraction of the four-momentum, then there must be some undetected hadrons somewhere which do carry it. The E802 Collaboration noted that an undetected excess of low-$p_\perp$ particles could result in a 25% enhancement of dN/dy over the exponentially fitted

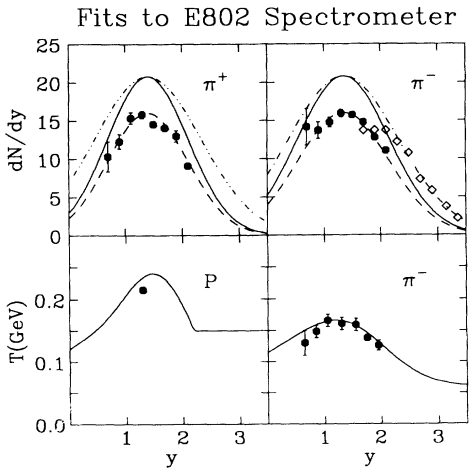

FIG. 5. Data as in Fig. 2 with E802 dN_{π^+}/dy [9] instead of protons. Also in the upper panels we show fit 1 (solid), fit 2 (solid), fit 3 (solid π^+ and dot-dashed π^-), and fit 4 (dot-dot-dashed π^+ and dot-dashed π^-). The lower panels show the $T(y)$ which were used for all of the fits.

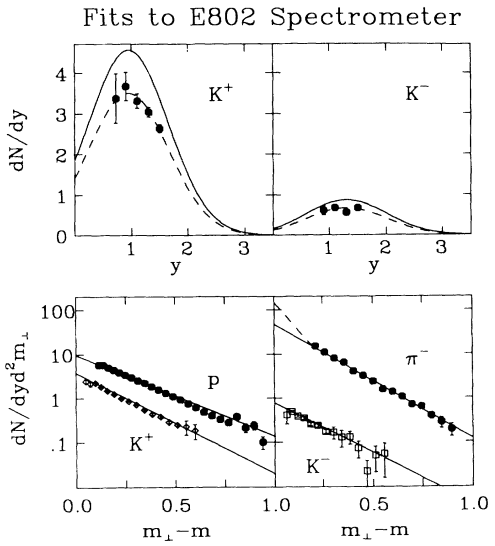

FIG. 6. The upper panels show the E802 $K^\pm$ rapidity distributions in central Si+Au reactions (solid dots), while the bottom panels show $m_\perp$ distributions for $y=1.3$ in these same reactions [9]. Simple fits to the data are shown by dashed curves in the upper panels and solid lines in the lower panels. The solid curves in the upper panels show the 30% enhancement used in fit 1–fit 4. The dashed line in the lower right panel shows a low $m_\perp$ component which would give rise to a 30% systematic error in dN_π/dy.

data [9]. To take this into account as well as other possible systematic errors in the data, we multiply each of our $(dN/dy)_i$ functions by $\alpha=1.3$ and adjust $C_{\rm pro}$ to 2.3 in order to preserve high-rapidity agreement with E810 and E814 ($C_{\rm spec}=43.9$ for charge conservation). Even with this 30% enhancement over all of the E802 data, we find that 50 GeV/c of momentum and 45 GeV of energy are still missing.

It seems that either the true dN_i/dy exceed the published E802 data by more than 30% in some rapidity regions or else the "missing" four-momentum must be carried by more high-rapidity hadrons than we use in the above extrapolations. If we assume that the latter is true, then the least transparent solution which does not overpredict any of the spectrometer data by more than 30% has fit 1=(2.75,3.4,40.9,01.7), where now a constant n/p ratio of 1.46 is assumed throughout and $(\alpha,\delta_{\rm pro})=(1.3,0.25)$ for the rest of the fits considered in this paper. This four-momentum conserving fit (solid lines in Figs. 4–6) overpredicts high-rapidity E810 and E814 proton data by a factor of 2. By allowing a 50% disagreement with the last proton data point, a slightly less transparent solution can be found: fit 2=(2.5,4.29,32.28,0.25), which only overpredicts E810 and E814 by 50% (dot-dashed curve in Fig. 4). These solutions have 10.8 and 10.1 nucleons, respectively, in the projectile region ($2.44<y<3.5$). In the lower half of Fig. 6 we show how an undetected low-$m_\perp$ component for pions could give rise to a 30% normalization error in dN_π/dy. However, since a high-$m_\perp$ hadron with rapidity y carries more four-momentum than a low-$m_\perp$ hadron with the same rapidity, it is more conservative to use a uniform 30% enhancement everywhere as we did in our calculations.

If we allow a 40% disagreement with the last two E802 π^- data points, the width of the dN_{π^-}/dy Gaussian can be increased to $\delta_{\pi^-}=1.85$ to provide agreement with E810 negatives at high rapidities (dot-dashed dN_π/dy in Fig. 5). By using fit 3=(2.5,4.58,72.7,0.07) to define the proton distribution, four-momentum can be conserved with 9.7 nucleons in the projectile region. The $y>0$ protons in this fit are distributed almost identically to the protons in fit 2, though from charge conservation the enhanced number of π^-'s causes a smaller n/p ratio (=1.33). Finally, from the fact that silicon is isosymmetric, one could argue that high-rapidity pions should be isosymmetric and therefore that the π^+'s should also be distributed like the E810 negatives at high rapidities. This can be achieved by taking $\delta_{\pi^+}=1.75$ and fit 4=(2.5,1.92,49.3,0.90), which has only 6.6 nucleons in the projectile region and is shown by the dot-dot-dashed dN_p/dy and dN_π/dy curves in Figs. 4 and 5. Though this fit conserved four-momentum and agrees well with high-rapidity E810 and E814 proton data, it disagrees with the last two E802 π^+ data points by 70–100 % and it features an n/p ratio of 1.56 even in the projectile region.

It is instructive to compare the four fits discussed above to other preliminary data from E802 as well as to leading neutron data from E814. In addition to the spectrometer arm, E802 has a target multiplicity array (TMA) detector which measures $dN/d\eta$ of charged particles and a beam calorimeter (ZCAL) which measures the residual beam energy after a collision. Due to the geometry of the ZCAL detector, there is some uncertainty as to whether it measures the energy of final particles with $\theta<0.8°$ or with $\theta<2.2°$ [13]. For $\theta_{\rm max}=0.8°$ the four fits discussed above give ZCAL energies (in GeV) of (5.3,3.8,4.4,4.1), while for $\theta_{\rm max}=2.2°$ these same fits give (37.0,27.4,30.6,27.6). If $\theta_{\rm max}$ is indeed 0.8°, then none of the above fits are inconsistent with correlations between the TMA (which defines the central trigger) and ZCAL measurements [13]. In Fig. 7 we compare $dN/d\eta$ distributions from the four fits and RQMD [17] with preliminary TMA data [10]. It is interesting that the four fits, each of which exceed the spectrometer multiplicities by at least 30%, still underestimate the TMA multiplicity. RQMD, on the other hand, can reproduce $dN/d\eta$ quite well even though it overpredicts spectrometer yields by 50–70 % in some rapidity regions. Since no reasonable fit or model can simultaneously reproduce both the spectrometer and TMA charged particle multiplicities, there appears to be some inconsistency between these two data sets. We note here that preliminary E814 $dN/d\eta$ data are in very good agreement with the E802 TMA data [30].

In the E814 experiment, neutrons emerging from Si+Pb collisions with a beam angle of $\theta<0.8°$ are measured using a forward spectrometer [12]. Their rapidity is determined by the amount of energy that they deposit in the spectrometer, and so a dN_θ/dy plot of neutrons having $\theta<0.8°$ is generated. In Fig. 8 we compare dN_θ/dy from our four fits with leading neutron data for central ($\sigma\sim40$ mb) Si+Pb collisions [12]. The agreement is best for fit 4, but due to the statistical uncertainty of the data as well as the different target (Pb) and trigger used by E814, none of the fits can be ruled out. In addi-

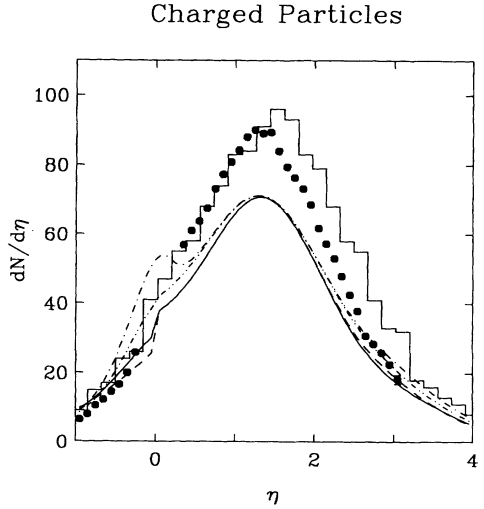

FIG. 7. Preliminary $dN_{\rm ch}/d\eta$ data [10] are compared to results of RQMD [17] (histogram), fit 1 (solid), fit 2 (dashed), fit 3 (dot-dashed), and fit 4 (dot-dot-dashed).

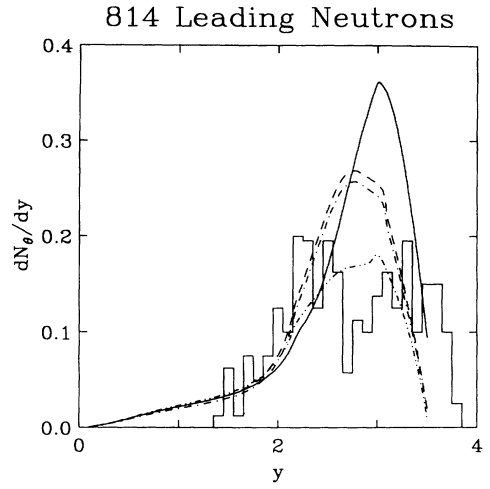

FIG. 8. The histogram shows the rapidity distribution for neutrons emerging with a beam angle of less than 0.8° in central ($E_{1814} > 13$ GeV) Si+Pb collisions [12]. Fit 1 (solid), fit 2 (dashed), fit 3 (dot-dashed), and fit 4 (dot-dot-dashed) for central Si+Au are compared to these data.

tion to leading neutrons, E814 also measures $dE/d\theta$ [31]. Though these data are not yet published, we have plotted $dE/d\theta$ predictions for our four fits and Attila in Fig. 9. It will be very interesting to see how the E814 data compare to these predictions, since for $5° < \theta < 15°$ $dE/d\theta$ is sensitive to the differences in the projectile region between the Attila model and our model-independent fits.

It should be emphasized that the four fits are conservative in that each assumes that all of the E802 spectrometer data are systematically low by at least 30%. There are, of course, other less transparent solutions which are consistent both with the spectrometer data and with conservation laws. For example, abnormally large numbers of π^0's, photons, or high-energy electrons could be produced in these collisions without being detected by the spectrometer. These solutions, however, imply bizarre and unprecedented physics. The four fits discussed above are thus the least unusual solutions which are more or less consistent with the reported E802 spectrometer data. One might argue that simplest solution of all to the problem of "missing" momentum is that the E802 spectrometer data are systematically low by 20–40 % at low rapidities and by 40–70 % at high rapidities. If that were the case, then a number of conventional models would be able to reproduce both the spectrometer dN/dy and the TMA $dN/d\eta$ data reasonable well. If the spectrometer data do in fact have such large systematic errors for central Si+Au collisions, then one might expect similar errors to be present in central Si+Al data, where the extrapolation to projectile rapidities is more accurately known from the approximate symmetry of the projectile and target. However, Bloomer performed an analysis using symmetric functions in which he found that energy conservation together with ZCAL data implied that the total systematic errors of the spectrometer data were less than 20% for central Si+Al collisions [13]. We are led to conclude either that new systematic errors are present in central Si+Au collisions or that some new and unexpected physics occurs (i.e., anomalously large neutral particle production, or large numbers of final particles in the projectile region).

For the remainder of this paper, we take the normalization of the E802 spectrometer data at face value, ignoring the E810 and E814 data. None of the models which we have considered in this paper are consistent with the normalization of the spectrometer data; therefore, those models cannot be used to assess the stopping power implied by these data. For that purpose we now construct hybrid models that can reproduce the reported E802 data. It should be emphasized that these models will *not* be able to simultaneously reproduce high-rapidity E810 and E814 data for reasons of momentum conservation as demonstrated above.

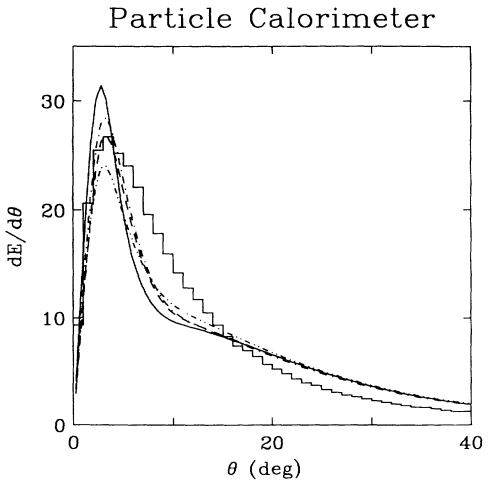

FIG. 9. Angular energy distributions (kinetic energy for baryons) are shown for Attila [26] (histogram), fit 1 (solid), fit 2 (dashed), fit 3 (dot-dashed), and fit 4 (dot-dot-dashed).

V. HYBRID MODELS

The most straightforward way to generalize the firestreak model to incorporate transparency is to assume that each tube-tube interaction produces two firestreaks (projectile and target) rather than one. We must then determine the rapidity (y_i) and rest energy per baryon (M_i^*) for each of these streaks. In order to treat projectile and target consistently, we must either pick y_p and y_t or M_p^* and M_t^*, since the remaining two can be solved for by energy and momentum conservation. A simple linear parametrization of the projectile and target streak rapidities is given by

$$y_p = y_{p0} - \left[\frac{N_t}{N_0}\right]\left[\frac{\sigma_{\rm in}}{a_\perp}\right], \qquad y_t = \left[\frac{N_p}{N_0}\right]\left[\frac{\sigma_{\rm in}}{a_\perp}\right], \tag{15}$$

where N_0 is the number of nucleons in a tube of size $a_\perp = \sigma_{\rm in} = 30$ mb necessary to cause a one unit rapidity

shift of the opposing tube. The last factor in each of the above equations was included to insure that the stopping power would be independent of the lattice size ($a_\perp$) chosen. Unfortunately, the above prescription leads to a number of cases where M^* of one of the fireballs is forced by four-momentum conservation to be less than the mass of the nucleon. Figure 10 shows the regions of (N_p,N_t) space for which this problem arises. Similar problems were encountered with other parametrizations in which y_p and y_t were chosen independently.

These problem regimes could in principle be handled specially by demanding complete transparency or the formation of a single fireball, but we chose instead to utilize a different algorithm which avoids special cases. First, in the center-of-mass frame of two colliding tubes containing N_p and N_t nucleons, the incoming momentum, P^*, is found. Next, the momentum of each tube is reduced by an amount proportional to the number of binary collisions, N_pN_t:

$$\Delta P^* = \delta p_z N_p N_t \left[\frac{\sigma_{\text{in}}}{a_\perp}\right] . \tag{16}$$

Finally, the energy/baryon is required to be the same for both of the outgoing firestreaks ($M_p^* = M_t^* = M^*$). M^* and the c.m. firestreak rapidities y_p^* and y_t^* can then be found from the following equations:

$$M^* N_p \sinh(y_p^*) = M^* N_t \sinh(y_t^*) = P^* - \Delta P^* , \tag{17}$$

$$M^* N_p \cosh(y_p^*) + M^* N_t \cosh(y_t^*) = M_{\text{c.m.}}(N_p + N_t) , \tag{18}$$

where the c.m. energy/baryon of the tube-tube system, $M_{\text{c.m.}}$, is determined by kinematics. Due to the symmetries of this method, M^* monotonically increases from m_N to $M_{\text{c.m.}}$ as ΔP^* is increased from 0 to P^*. When the prescription of (16) gives a $\Delta P^* \geq P^*$, a single firestreak with $M^* = M_{\text{c.m.}}$ and $y_p^* = y_t^* = 0$ is assumed to be formed. Defining the effective nuclear thickness, z_i, via $N_i = a_\perp \rho_0 z_i$, the momentum shift per baryon of the projectile (target) is thus assumed to increase linearly with the effective target (projectile) thickness. The nuclear stopping power of this model is controlled by a single parameter—the momentum loss per binary collision δp_z, or equivalently, the nuclear stopping length

$$L_s = m_N \sinh(y_{p0}/2)/(\sigma_{\text{in}} \rho_0 \delta p_z) . \tag{19}$$

The meaning of this stopping length can be most easily seen in symmetric collisions ($z_p = z_t = z$), where the fractional momentum loss ($\Delta P^*/P^* = z/L_s$) increases linearly and reaches unity when $z = L_s$. Thus a stopping length of 10 fm implies that two colliding tubes of length 10 fm will just be able to stop each other.

In Fig. 11 we compare models with various values of L_s to the data ($\rho_{\text{fr}} = 2\rho_0$ and $\gamma_s = 0.7$ have been chosen to provide the best agreement with kaon data and pion temperatures). Compared to the data, $L_s = 10$ fm is evidently too small and $L_s = 26$ fm is too large. Though $L_s = 17$ fm provides good agreement to all but the last point of the dN_p/dy data, its pion peak is shifted to low rapidities, and its proton temperature is too low with a dip at midrapidity which is not seen in preliminary, unpublished $T_p(y)$ data [13]. It should be noted that folding the E802 spectrometer acceptance [22] into the double firestreak leads to less than a 10% suppression of the pion yield and no discernible change in the proton rapidity spectrum. This double firestreak description provides far better agreement with the data than any of the other models discussed so far, but in order to quantitatively reproduce all the features of the E802 data, further refinements are needed.

One of the key observations of E802 is that the transverse momentum slopes of protons and pions differ significantly. Therefore the amount of energy locked into transverse motion differs from that expected in simple

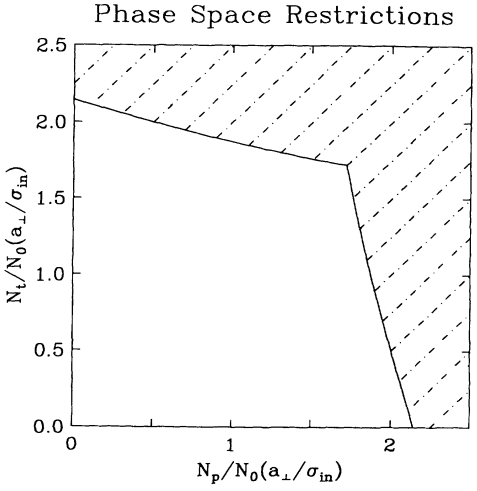

FIG. 10. The available phase space for the stopping prescription of Eq. (15) is shown by the unshaded region. In the shaded region, one or both of the receding fireballs must have a mass/baryon <0.939 GeV in order to conserve four-momentum.

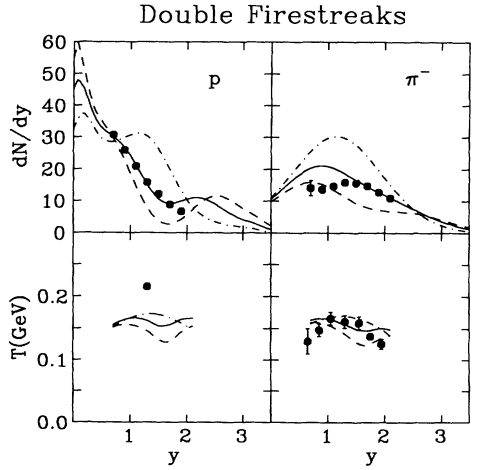

FIG. 11. Double firestreaks with $L_s = 10$ fm (dot-dashed), 17 fm (solid), and 26 fm (dashed) are compared to the data of Fig. 2.

thermal models with one freeze-out temperature. Collective flow [18] provides one natural mechanism for different slopes. Different freeze-out criteria due to different cross sections provides another. To test the effect of this difference on the conclusion of the stopping power, we developed a more complex multicomponent model (mcm). The details of this model are given in the Appendix. We emphasize that the mcm is not meant to be a realistic model of the physics, but a convenient numerical tool to help sort the implications of various features of the data.

In Figs. 12 and 13 we show two mcm solutions. The solid line is the best fit to the data (mcm1), with $L_s = L_s' = 26$ fm, $M_2^* = 1.4$ GeV, $M_2^* = 1.85$ GeV, $\rho_{\rm fr} = \rho_0$, $T_{\rm mes} = 160$ MeV, and $\gamma_s = 0.25$. This is the fit that was used by us in Ref. [8]. The dashed curve is another fit to the data (mcm2) with $L_s = 20$ fm, $L_s' = 50$ fm, $M_1^* = 1.55$ GeV, $M_2^* = 2$ GeV, $\rho_{\rm fr} = \rho_0$, $T_{\rm mes} = 165$ MeV, and $\gamma_s = 0.25$. The dot-dashed curve for the pions shows mcm1 with the spectrometer acceptance [22] folded in. Due to the many adjustable parameters of this model, both mcm1 and mcm2 are able to quantitatively reproduce almost all of the E802 spectrometer data. The most notable discrepancy is the 25% overprediction of low-rapidity pions by these models after the experimental acceptance has been taken into account. Unlike the models discussed previously which also overpredict pions, the disagreement of the mcm fits is much smaller and only seen at low rapidity. Both of the mcm fits as well as the $L_s = 17$ double firestreak exhibit the high degree of nuclear transparency necessary to be able to reproduce the E802 spectrometer data.

The $L_s = 17$ double firestreak as well as mcm1 and mcm2 discussed above have all had their parameters tuned to best fit the E802 central Si+Au spectrometer data. The quality of these fits is therefore not very surprising, especially in the case of the mcm where there

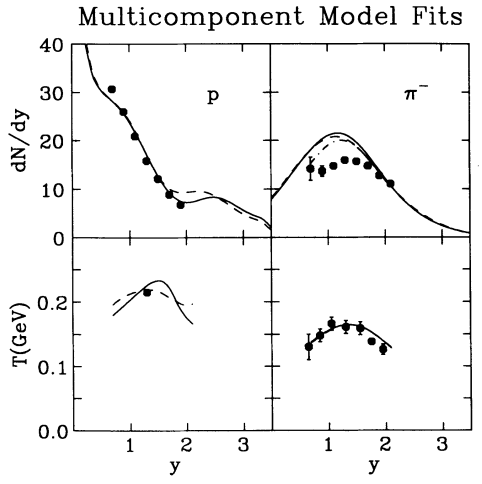

FIG. 12. Multicomponent model fits mcm1 (solid) and mcm2 (dashed) are compared to the data of Fig. 2. The dot-dashed curve for the pions shows the result of mcm1 with the experimental acceptance taken into account [22].

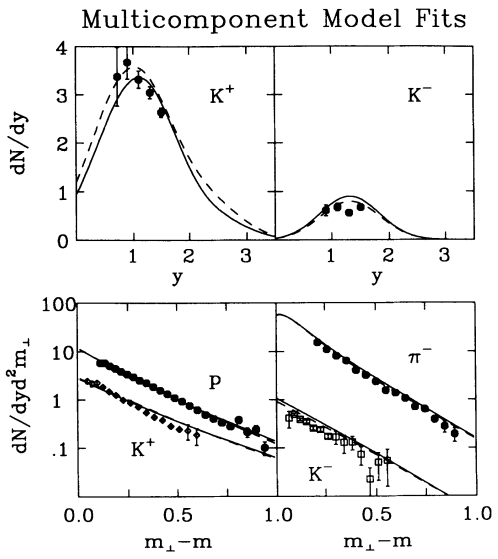

FIG. 13. Multicomponent model fits mcm 1 (solid) and mcm2 (dashed) are compared to the data of Fig. 6.

are so many free parameters. An interesting test of these models is to see how well they can reproduce unpublished E802 central Si+Al and Si+Cu data [13]. For these reactions, there is very little difference between the results of mcm1 and mcm2; both of them are able to reproduce dN_π/dy and midrapidity dN_p/dy of both collisions to within 20%. Both parameter sets predict too many target protons, but this could be due to large fragment formation in these reactions. The $L_s = 17$ double firestreak obtains results similar to mcm1 and mcm2 for Si+Cu, but it exhibits a factor of 2 too few midrapidity protons and pions in central Si+Al collisions. Even though the double firestreak uses a smaller value for L_s than the mcm fits, it exhibits less stopping when applied to lighter nuclei. This is because there is no center-of-mass firestreak in the double firestreak model, so a lot of energy is carried away by receding mesons. This effect becomes much more pronounced with less stopping (lighter nuclei). It should be noted that we were not able to find a model which could simultaneously fit E802 $p+A$ data and central $A+B$ data. However, to the extent that central Au+Au reactions bear more similarity to central Si+A than to $p+A$ reactions, the predictions for Au+Au by our mcm fits are better supported by the E802 spectrometer data than those of the models discussed in the first parts of this paper. In Fig. 14 we show Au+Au predictions by the $L_s = 10$ fm (dot-dot-dashed) and $L_s = 17$ fm (dot-dashed) double firestreaks as well as by the mcm fits (mcm1, solid; mcm2, short-dashed). For such large nuclei, the $L_s = 10$ fm double firestreak forms essentially a fully stopped firestreak which consequently features a much narrower and higher peak in dN_p/dy than the other models. This is due to the fact that full stopping has not been achieved in these models, as can be easily seen by looking at the long-dashed line which represents the projectile proton rapidity distribution of

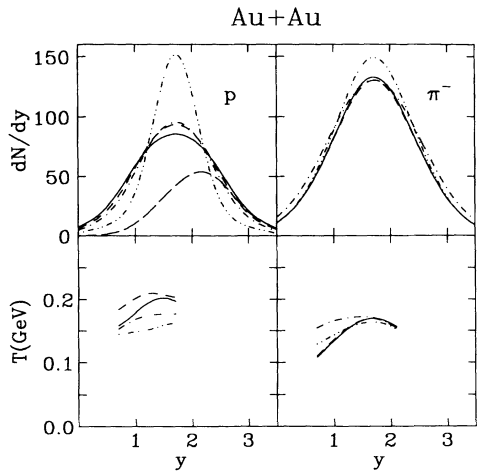

FIG. 14. Predictions for central ($0<b<3$ fm) Au+Au collisions by multicomponent model fits mcm1 (solid), mcm2 (dashed), and double firestreaks with $L_s=10$ fm (dot-dot-dashed) and $L_s=17$ fm (dot-dashed). Projectile protons for mcm1 are shown by the long-dashed curve in the upper left panel.

mcm1. Since Au+Au is symmetric, the projectile and target contributions combine to form a symmetric, Gaussian-like dN_p/dy which would be difficult to differentiate from the result that one would get from a fully stopped fireball undergoing longitudinal expansion. For asymmetric collisions like Si+Au, on the other hand, these two cases can be clearly distinguished. For this reason it is important to study and understand asymmetric as well as symmetric collisions.

VI. CONCLUSION

We showed that none of the present models which assume complete nuclear stopping and none of the present nonequilibrium string models are consistent with the published E802 spectrometer data [9] for central Si+Au reactions. For example, even the RQMD model is not consistent with these data, as they note that "the problem of the 'missing' energy-momentum could be resolved if the normalization of the E802 spectrometer data were too small" [28]. If corrections to the normalization nowhere exceed 30%, then energy-momentum and baryon conservation alone require the existence of at least 10–11 nucleons in the projectile region ($y>2.44$) which, however, would be inconsistent with E810 [11] and E814 [12] results. The fact that the high-rapidity E810 and E814 proton data are in excellent agreement, even though the E810 trigger is less central and the E814 trigger is more central than E802, makes it unlikely that the discrepancies of those data with fits to the E802 spectrometer are due to triggering effects alone. A double firestreak and a multicomponent model have been developed to quantify the degree of transparency needed to reproduce the spectrometer data, and nuclear stopping lengths of 17–26 fm were found. These lengths are much larger than the lengths of 8–10 fm which were expected based on other experiments at these and higher energies [14]. On the other hand, the high-rapidity data from E810 and E814 as well as preliminary $dN/d\eta$ data from E802 [10] and E814 [30] are consistent with models incorporating the expected degree of nuclear stopping. Until the discrepancies between all data sets are resolved, conclusions about full nuclear stopping remain premature.

ACKNOWLEDGMENTS

We are especially grateful to Matt Bloomer, Shoji Nagamiya, Flemming Videbaek, Sam Lindenbaum, and Johanna Stachel for extensive discussions on the AGS data. This work was supported by the Office of Energy Research, Division of Nuclear Physics of the Office of High Energy and Nuclear Physics of the U.S. Department of Energy under Contract No. DE-AC03-76SF00098.

APPENDIX

In the multicomponent model, we decompose a single fireball into two with two different freeze-out times (one baryonic and one mesonic). Baryonic fireballs are assumed to consist of baryons (no antibaryons), K^+'s and K^0's balanced such that they have zero net strangeness. Since the baryon resonsances are allowed to decay as usual, there are some pions which are produced by baryonic fireballs. Mesonic fireballs are comprised of all hadronic resonances (including baryons), but have zero baryon number and strangeness. We suppose that each tube-tube collision gives rise to one fully stopped, double-freeze-out firestreak at the local center of mass as well as to receding projectile and target baryonic firestreaks. A number of new parameters must be introduced into this model to determine the energy and baryon number of each of the firestreaks involved.

First, as in the double firestreak, a value of L_s is specified in order to determine M^*, y_p^*, and y_t^* for the receding firestreaks. Second, another stopping length, L_s', is chosen in order to determine the fraction of baryons from each tube which get fully stopped:

$$f_s=(z_p z_t)^{1/2}/L_s' \ . \tag{A1}$$

Next, if the initial c.m. energy/baryon, $M_{\text{c.m.}}$, of the tube-tube system is greater than an excitation mass parameter M_2^*, then the energy/baryon of the baryonic part of the central fireball is limited to $M_c^*=M_2^*$, and the energy/baryon available to the receding streaks becomes

$$M^*\rightarrow M^{*\prime}=\frac{1-f_s(M_2^*/M_{\text{c.m.}})}{1-f_s}M^* \tag{A2}$$

in order to conserve energy. If, on the other hand, $M_{\text{c.m.}}\le M_2^*$, then $M_c^*=M_{\text{c.m.}}$ and $M^{*\prime}=M^*$. If $M^{*\prime}$ turns out to be smaller than another parameter M_1^*, then there is no mesonic firestreak at all, and the tube-tube interaction is modeled by three purely baryonic streaks. However, if $M^{*\prime}>M_1^*$ then the receding streaks have their energy/baryon limited to M_1^* ($M_p^*=M_t^*=M_1^*$), and a mesonic streak overlapping the c.m. baryonic

streak is created with energy

$$E_{\rm mes}=(M^{*\prime}-M_1^*)(1-f_s)\times[N_p\cosh(y_p^*)+N_t\cosh(y_t^*)]\ . \quad \text{(A3)}$$

For the mesonic streaks, a freeze-out temperature $T_{\rm mes}$ is specified and $V_{\rm fr}$ is solved for trivially, since $\mu=\mu_s=0$ for streaks with zero baryon number and strangeness. Note that if $(z_p z_t)^{1/2}\geq L_s'$ or $\Delta P^*\geq P^*$ for any two incoming tubes, then this model reduces to a fully stopped firestreak with separate baryonic and mesonic freezeout criteria.

The many parameters of this model have interrelated effects but can be approximately explained as follows. The amount of baryon stopping is controlled by L_s and L_s'. The central ($1.1<y<1.7$) values of $T_p(y)$ are controlled by L_s', M_2^*, and $\rho_{\rm fr}$, while the wings ($y<1.1, y>1.7$) of $T_p(y)$ are controlled by M_1^* and $\rho_{\rm fr}$. It should be noted that for baryonic firestreaks with M_i^* fixed, decreasing $\rho_{\rm fr}$ cools the baryons by forcing them into higher mass resonances. $T_\pi(y)$ is mainly controlled by $T_{\rm mes}$, though $\rho_{\rm fr}$, M_1^*, and M_2^* also have effects by adjusting the number of cool pions coming from baryon resonances. The height of dN_π/dy is affected by all of the parameters; increasing the value of any one of them leads to a decrease in the number of pions. The overall number of kaons is adjusted by γ_s, while the K^+/K^- ratio is determined by the number of strange baryons, which is again a function of $\rho_{\rm fr}$, M_1^*, and M_2^*.

[1] T. Abbott *et al.*, E802 Collaboration, Phys. Lett. B **197**, 285 (1987).
[2] M. S. Tannenbaum *et al.*, Nucl. Phys. **A488**, 555c (1985).
[3] P. Braun-Munzinger *et al.*, Z. Phys. C **38**, 45 (1988).
[4] J. Stachel, Nucl. Phys. **A527**, 167c (1991).
[5] J. Satchel and P. Braun-Munziner, Phys. Lett. B **216**, 1 (1989); Nucl. Phys. **A498**, 577c (1989).
[6] E. F. Staubo *et al.*, Phys. Lett. B **229**, 351 (1989).
[7] N. S. Amelin *et al.*, Phys. Rev. C **44**, 1541 (1991).
[8] S. Chapman and M. Gyulassy, Phys. Rev. Lett. **67**, 1210 (1991).
[9] T. Abbott *et al.*, E802 Collaboration, Phys. Rev. Lett. **64**, 847 (1990); **66**, 1567 (1991).
[10] F. Videbaek, in *Proceedings of the Workshop on Heavy Ion Physics at the AGS, 1990,* edited by Ole Hansen in BNL Report No. BNL-44911, 1990 (unpublished); and private communication with F. Videbaek.
[11] W. A. Love *et al.*, E810 Collaboration, Nucl. Phys. **A525**, 601c (1991).
[12] J. Barrette *et al.*, E814 Collaboration, Phys. Rev. Lett. **64**, 1219 (1990); P. Braun-Munziner, Proceedings of Quark Matter '91, 1991 (unpublished).
[13] M. A. Bloomer, MIT Ph.D. thesis, 1990; and private communication.
[14] W. Busza and R. Ledoux, Annu. Rev. Nucl. Part. Sci. **38**, 119 (1988); S. Date, M. Gyulassy, and H. Sumiyoshi, Phys. Rev. D **32**, 619 (1985).
[15] H. Sorge *et al.*, Nucl. Phys. **A525**, 95c (1991).
[16] H. Sorge *et al.*, UFTP Report No. 263, 1991.
[17] R. Mattiello *et al.*, Phys. Rev. Lett. **63**, 1459 (1989).
[18] G. Brown *et al.*, Phys. Rev. C **43**, 1881 (1991); C. M. Ko *et al.*, Phys. Rev. Lett. **66**, 2577 (1991).
[19] C. M. Ko *et al.*, Phys. Rev. Lett. **67**, 1811(E) (1991).
[20] J. Gosset, J. Kapusta, and G. D. Westfall, Phys. Rev. C **18**, 844 (1978).
[21] S. Das Gupta and A. Z. Mekjian, Phys. Rep. **72**, 131 (1981).
[22] T. Abbott *et al.*, E802 Collaboration, Z. Phys. C **38**, 135 (1988).
[23] S. Nagamiya, Proceedings of Quark Matter '91, 1991 [12].
[24] W. D. Myers, Nucl. Phys. **A296**, 177 (1978).
[25] B. Andersson *et al.*, Nucl. Phys. **B281**, 289 (1987).
[26] M. Gyulassy, CERN Report No. CERN-TH.4794, 1987; in Proceedings of the Balatonfured Conference on Nuclear Physics, 1987 (unpublished).
[27] F. Videbaek, in *Proceedings of the International Symposium on High Energy Nuclear Collisions and Quark Gluon Plasma, Kyoto, Japan, 1991,* edited by M. Biyajima *et al.* (World Scientific, Singapore, 1992), p. 55.
[28] H. Sorge *et al.*, Phys. Rev. Lett. **68**, 286 (1992).
[29] J. Stachel, private communication.
[30] W. E. Cleland *et al.*, Nucl. Phys. **A525**, 91c (1991).
[31] D. Fox, private communication.